Pseudorange Multipath at Zomba Geodynamics Continuously Operating Reference Station (CORS) in Malawi

Robert S.B. Galatiya Suya[1], Mphatso Soko[2], Harvey Chilembwe, Charles C. Kapachika, Chikondi Mphamba

Department of Geomatics, Faculty of the Built Environment,
University of Malawi-The Polytechnic, P/Bag 303, Chichiri, Blantyre 3, Malawi.

rsuya@poly.ac.mw[1] ; msoko@poly.ac.mw[2]

Abstract

Multipath effects are mostly regarded as a nuisance in Global Navigation Satellite System (GNSS) receiver measurements and it is of utmost relevance to expose the magnitude this error has on observations. The impact of multipath is characterized in the context of a given environment and application. In Malawi, Zomba geodynamics Continuously Operating Reference Station (CORS) is in a multipath prone environment. The GNSS observations for this station have been used in geodynamics studies in Malawi without an understanding of multipath affecting the positioning accuracy. Taking this as an advantage, this paper evaluated pseudorange multipath (MP) and signal noise ratio (SNR) on both L1 (MP1 and SNR1) and L2 (MP2 and SNR2) for the station. This was specifically addressed by computing the elevation mask with minimum and maximum multipath effects. In addition, the number of satellite vehicles (SVs) and their associated Geometric Dilution of Precision (GDOP) are also determined to define their relationship with respect to elevation angles. One week GNSS observations spanning a twenty-four hour interval for DOY 001 to DOY 007 in January 2018 were analysed in Translation Editing and Quality Check (TEQC) software at four (10º, 15º, 20º and 25º) cut-off angles. Results indicate high multipath effects for both MP1 and MP2 at 10º elevation mask among the four elevation masks. The least MP1 and MP2 multipath effects were detected at an elevation angle of 25º. In addition, MP1 multipath was worse than MP2 all the angles. Moreover, statistical results demonstrated an increase in both SNR1 and SNR2 with respect to elevation angle. For these days, L2 signal was more affected by noise than L1. Further to this, an assessment of SVs and GDOP for the CORS show that at least ten (10) satellites were observed in each day at 10º and 15º elevation cut-off. The number of satellites dropped to five (5) at the elevation angle of 25º resulting into a larger GDOP value of 4.5 (a decrease by about 38% from 1.7 at 10º and 15º elevation cut-off angles). Therefore, to increase both the number of satellites and precision, Zomba CORS may be upgraded to a multi-constellation CORS by including other navigation systems such as GLONASS, Galileo and BeiDou. While it is possible to reject GNSS satellite observations below the horizon, it is recommended that post-processing of GNSS data for Zomba geodynamics CORS be done at elevation masks above 15º. Considering that multipath repeats itself every sidereal

day, it is thus recommended to model or remove multipath affecting Zomba geodynamics CORS. In addition, the study also recommends that trees very close to Zomba CORS antenna be removed to reduce signal scattering.

Keywords: *Pseudorange Multipath, Signal-Noise-Ratio, Satellite Vehicles, Geometric Dilution of Precision.*

1. Introduction

Multipath propagation is one of the limiting factors to both pseudorange and carrier phase-based positioning. Satellite signals have to reach the Global Navigation Satellite System (GNSS) antenna through a direct line-of-sight (LOS). Multipath phenomena occurs when the electromagnetic signals arrive at the antenna through multiple paths, non LOS paths (Hsu et al., 2015). Multipath can increase or decrease the measured pseudoranges based on the vicinity of the GNSS antenna (Webb, 1997). Multipath effect reaches up to about 5 cm and as high as a few tens of meters in carrier phase and pseudorange GNSS positioning, respectively (Hofmann-Wellenhof et al., 1994).

The resultant range errors caused by multipath vary depending on satellite geometry (Phan, Tan, & McLoughlin, 2013), reflecting surfaces (Preston, 2015) and the GNSS antenna design (Yuan et al., 2017). Antenna mounted on roof tops are susceptible to multipath (Kildal, Orlenius, & Carlsson, 2012) due to vents and other reflective objects within the field of view (Leick, Rapoport, & Tatarnikov, 2015). Furthermore, soil moisture have proved to degrade the phase of not only signal-to-noise ratio (SNR) modulation pattern but also of its magnitude (Zavorotny et al., 2010). An in-depth insight on multipath phase rates in different multipath environments can be found in Irsigler (2010).

The variations and causes of multipath have motivated research in multipath detection and mitigation techniques. This has consequently resulted into the classification of multipath mitigation techniques into hardware-(Philippov et al., 2019; Krantz & Riley, 1990), site- (Lau & Cross, 2007) and algorithm-dependent (Preston, 2015; Wieser & Brunner, 2002). The former describe the state-of-the-art choke-ring and Trimble's Zephyr antennas which mitigate multipath by minimising the gain of a low-elevation signal. Recent studies in multipath mitigation techniques have also assisted researchers to undertake feasibility studies to aid proper selection of antenna for Continuously Operating Reference Station (CORS) (Munghemezulu et al., 2016).

To unveil the least and most affected sites in the CORS network, Hilla & Cline (2004) evaluated the amount of pseudorange multipath occurring at over 390 National CORS network. In an integrated study of Global Positioning System (GPS) antenna for CORS and the International Global Navigation Satellite System (GNSS) Service (IGS) network, Park, et al.(2004) recommended choke-ring antenna in supressing multipath. To improve user location positioning performance, Dammalage (2017) proposed the application of real-time Differential GPS (DGPS) corrections to permanent reference stations. This is so because, the accuracy of a receiver position relies on the combination of site-dependent errors such as multipath, receiver clock error, and measurement noises (Lakmal, 2018). In

addition to these errors, the receiver position errors are also associated with atmospheric effects, and geometric dilution of precision effect.

Pseudorange multipath has an impact on both availability and integrity of GNSS-based positioning, navigation and timing (PNT)(Yuan et al., 2017). Multipath effect degrades the accuracy of navigation and positioning (Lentmaier et al. 2007). One of the weaknesses of pseudorange multipath is that it cannot be compensated for by observations provided by monitoring datasets (Kaplan and Hegarty, 2006). Worse still, it is still difficult to eliminate pseudorange multipath in precise PNT.

Different countries all over the world have CORS for both real-time and post-processing applications. Some of these functions are summarised in Abidin et al. (2010). Malawi has a geodynamics CORS installed at Zomba Geological Survey Headquarters. The station is installed at the roof-top and it records GNSS observations that are available for geodynamics studies in post-processing mode, in Malawi. Multipath is time and location dependent. Zomba geodynamics CORS is in a multipath prone environment. However, since its installation, no study has been conducted to evaluate the pseudorange multipath affecting the station. In this paper, pseudorange multipath and Signal Noise Ratio (SNR) are evaluated for this station at different elevation cut-off angles. This is done to identify the elevation mask with minimum multipath effects. The number of satellite vehicles (SVs) and their associated Geometric Dilution of Precision (GDOP) are also determined to define their relationship with respect to elevation angles.

2. Estimation of Parameters

2.1. Pseudorange Multipath Model

To evaluate pseudorange multipath at Zomba geodynamics CORS, Translation Editing and Quality Check (TEQC) software was used (Estey and Meertens, 1999). TEQC is a GNSS comprehensive toolkit with capability of computing the pseudorange multipath (MP) on L1 and L2 (i.e.: MP1 and MP2). This software utilises both pseudorange and carrier phase observables to eliminate the effects of satellite clocks, ionospheric delay, tropospheric delay, and station clocks.

For a satellite (k) and a receiver (i), the pseudorange and carrier phase measurements on L1 and L2 are given by:

$$P_{L1} = R + c\left(\Delta t^k - \Delta t_i\right) + I_{L1} + T + MP_{P1} \tag{1}$$

$$P_{L2} = R + c\left(\Delta t^k - \Delta t_i\right) + I_{L2} + T + MP_{P2} \tag{2}$$

$$\Phi_{L1} = R + c\left(\Delta t^k - \Delta t_i\right) + \lambda_{L1} N_{L1} - I_{L1} + T + MP_{\Phi_{L1}} \tag{3}$$

$$\Phi_{L2} = R + c\left(\Delta t^k - \Delta t_i\right) + \lambda_{L2} N_{L2} - I_{L2} + T + MP_{\Phi_{L2}} \tag{4}$$

In equations [1] to [4], P_1 and P_2 denote dual-frequency pseudorange observations in meters; Φ_{L1} and Φ_{L2} denote the carrier-phase observations on L_1 and L_2, respectively; R is the geometric distance

between satellite and receiver (in m); c is the speed of light in a vacuum (in m/s); Δt_i and Δt^k are the satellite and receiver clock corrections (in sec), respectively; I_{L1} and I_{L2} are the ionospheric range errors (in m); T is the tropospheric range error (in m); λ_{L1} and λ_{L2} denote the wavelengths of the signals on L_1 and L_2 which are approximately equal to 19 cm and 24 cm, respectively; $f_1 \approx 1.5754$ *GHz* and $f_2 \approx 1.2276$ *GHz* are the frequencies on signals L_1 and L_2, respectively; N_{L1} and N_{L2} integer ambiguities (cycles); MP_{P1}, MP_{P2}, $MP_{\Phi_{L1}}$ and $MP_{\Phi_{L2}}$ are the corresponding pseudorange and carrier phase multipath, respectively (including the observational noise).

The ionospheric delay for L_1 and L_2 is presented in [5] with $\alpha = \left(\dfrac{f_1}{f_2}\right)^2$:

$$I_{L2} = \alpha . I_{L1} \tag{5}$$

Subtract [4] from [3] then substitute [5] to yield [6]:

$$\frac{\Phi_{L1} - \Phi_{L2}}{[\alpha - 1]} = I_{L1} + \frac{\lambda_{L1} N_{L1} - \lambda_{L2} N_{L2}}{[\alpha - 1]} + \frac{MP_{\Phi_{L1}} - MP_{\Phi_{L2}}}{[\alpha - 1]} \tag{6}$$

To eliminate I_{L1}, simply combine [6] with [3], and this consequently results into [7]:

$$\begin{cases} \Phi_{L1} + \dfrac{\Phi_{L1} - \Phi_{L2}}{[\alpha - 1]} \equiv R + c\left[\Delta t^s - \Delta t_r\right] + T + \lambda_{L1} N_{L1} + \dfrac{\lambda_{L1} N_{L1} - \lambda_{L2} N_{L2}}{[\alpha - 1]} \\[2em] + MP_{\Phi_{L1}} + \dfrac{MP_{\Phi_{L1}} - MP_{\Phi_{L2}}}{[\alpha - 1]} = R + c\left[\Delta t^s - \Delta t_r\right] + T + b_1 + m_{\Phi_1} \end{cases} \tag{7}$$

The expression [7] is the linear combination of observed L_1 and L_2 carrier phases. In this equation, the ambiguity bias b_1 and phase multipath are introduced and expressed as [8] and [9], respectively:

$$b_1 = \lambda_{L1} N_{L1} + \frac{\lambda_{L1} N_{L1} - \lambda_{L2} N_{L2}}{[\alpha - 1]} \tag{8}$$

$$m_{\Phi_1} = MP_{\Phi_{L1}} + \frac{MP_{\Phi_{L1}} - MP_{\Phi_{L2}}}{[\alpha - 1]} \tag{9}$$

Combining [3], [6] and [7] yields [10]:

$$\begin{cases} P_{L1} - \left[1 + \dfrac{2}{(\alpha - 1)}\right]\Phi_{L1} + \left[1 + \dfrac{2}{(\alpha - 1)}\right]\Phi_{L2} = \\[2em] MP_{P1} - \dfrac{\lambda_{L1} N_{L1} - \lambda_{L2} N_{L2}}{[\alpha - 1]} - b_1 + MP_{\Phi_{L1}} - 2m_{\Phi_1} \end{cases} \tag{10}$$

Thus, the expression for the new ambiguity and new phase multipath effect are presented in [11] and [12], respectively:

$$\begin{cases} B_1 \equiv -\dfrac{\lambda_{L1} N_{L1} - \lambda_{L2} N_{L2}}{[\alpha - 1]} - b = -\left[1 + \dfrac{2}{(\alpha - 1)}\right]\lambda_{L1} N_{L1} + \\[2em] \left[1 + \dfrac{2}{(\alpha - 1)}\right]\lambda_{L2} N_{L2} \end{cases} \qquad [11]$$

$$\begin{cases} M_{\Phi 1} \equiv -\left[MP_{\Phi_{L1}} - MP_{\Phi_{L2}}\right] - m_{\Phi_1} = -\left[1 + \dfrac{2}{(\alpha - 1)}\right]MP_{\Phi_{L1}} \\[2em] + \left[1 + \dfrac{2}{(\alpha - 1)}\right]MP_{\Phi_{L2}} = MP_{\Phi_{L1}} - 2m_{\Phi_1} \end{cases} \qquad [12]$$

The pseudorange multipath on L_1 and L_2 are then defined from [10] as linear combinations in [13] and [14], respectively:

$$MP_{P1} \equiv P_{L1} - \left[1 + \frac{2}{(\alpha - 1)}\right]\Phi_{L1} + \left[1 + \frac{2}{(\alpha - 1)}\right]\Phi_{L2} = P_1 + B_1 + M_{\Phi_1} \qquad [13]$$

$$MP_{P2} \equiv P_{L2} - \left[\frac{2\alpha}{(\alpha - 1)}\right]\Phi_{L1} + \left[\frac{2\alpha}{(\alpha - 1)} - 1\right]\Phi_{L2} = P_2 + B_2 + M_{\Phi 2} \qquad [14]$$

where P_1 and P_2 are the pseudorange observations on L1 and L2 signal frequencies, respectively.

2.2.   Signal to Noise Ratio

SNR is a quantity of the ratio of the amplitude of the recovered GNSS carrier signal to the noise (Bilich, Larson, & Axelrad, 2004). SNR is used for assessing the performance of acquisition and tracking capabilities of a receiver (Joseph, 2010). In any receiver environment, SNR is computed by the inherent receiver's tracking algorithm as a composite of both direct LOS and indirect LOS (Bilich and Larson, 2007). In an environment susceptible to multipath, the absolute SNR is expressed according to [15], Bilich et al., (2007):

$$SNR \equiv A_d^2 + A_m^2 + 2A_d A_m \cos\varphi \qquad [15]$$

In equation [15], A_d is the amplitude of the direct signal; A_m is the amplitude of the reflected signal after code correlation, and φ is the relative phase difference between the reflected and direct signal.

2.3. Geometric Dilution of Precision

The accuracy of a navigation system has a strong correlation with the number of satellites tracked as well as satellite configuration. The satellite geometry provides either low or high dilution of precision (DOP) factors. DOP is used to quantify the degree to which satellite-user geometry dilutes point positioning accuracy. Optimal satellite arrangement in the sky leads to low DOP values. DOP is deduced from the diagonal elements of the cofactor matrix (Q). These elements are simply the variances that describe the North, East, Vertical (Up) and time DOP values, as expressed in [16], Leick et al. (2015):

$$Q = \begin{bmatrix} q_N & & & \\ & q_E & & \\ & & q_U & \\ & & & q_\xi \end{bmatrix} \qquad [16]$$

In [16], q_N, q_E, and q_U denote the DOP values for the North (N), East (E), Up (U) coordinates, respectively; and q_ξ denotes the time DOP estimate. The matrix in [16] is symmetrical and the off-diagonal elements are computed covariances when survey observations are correlated. In case of un-correlated observations, all the off-diagonal elements are zeros.

For the satellite and receiver positions expressed in N, E, and U, the square-root of the diagonal entries of the geometry matrix are the north DOP (NDOP); east DOP (EDOP), and vertical DOP (VDOP). Since GNSS does not only compute three-dimensional (3D) position solution but also time, then the covariance matrix also outputs time DOP (TDOP). Depending on user requirement, DOP values are sometimes fused to form two-dimensional (2D) horizontal positioning (HDOP); 3D position DOP (PDOP), and total geometry DOP (GDOP). GDOP represents the combined effect of the Positional Dilution of Precision (PDOP) and the Time Dilution of Precision (TDOP) and is expressed as [17].

$$GDOP = \left(q_N + q_E + q_U + q_\xi \right)^{\frac{1}{2}} \qquad [17]$$

3. Zomba Geodynamics CORS

Zomba geodynamics CORS, currently observed and managed by Pennsylvania State University (PSU), is the only CORS in the Southern Region of Malawi. By convention, GNSS stations are identified with four-character names. As such, Zomba CORS is defined as 'Zomb'. In this work, the names 'Zomba' and 'Zomb' are interchangeably used to define the CORS located in Zomba district. This station is equipped with a dual-frequency GNSS Trimble receiver which observes GPS data only. The receiver has a protective antenna cover, radome, which acts as a water-proof. Furthermore, Zomba CORS runs on Linux operating system and it operates as a stand-alone reference station. Table 1 and Figure 1 depict the station characteristics and spatial location for Zomb CORS, respectively.

Table 1: Station characteristics for Zomb geodynamics CORS.

Parameter	Description
Station Name	Zomb
Town	Zomba
Country	Malawi
Position (WGS 84)	S 15° 22' 33.05" E 35° 19' 30.46" 988.2244 m
Recent Configuration	22-August 2010 [00:00] to 20-June 2018 [21:32]
Antenna Model	TRM59800.00
Antenna Serial Number	4933353426
Antenna Radome	SCIT
Receiver Model	Trimble NETRS
Receiver Serial Number	4927175246
Receiver Firmware	1.2-4
Observation Interval	15 Seconds
Agency	Pennsylvania State University

KEY: In this table, SCIT denotes SCIGN (southern California integrated GPS network) tall radome.

NETRS denotes Network Reference Station; which is a dual-frequency GPS receiver. The values

in the square brankets denote time in hours and minutes.

KEY: The numbers 1 to 4 denote the CORS, Iron sheet, Tree, and Telecommunication Tower. This station is located at the roof-top of Zomba Geological Survey Headquarters.

Figure 1: Zomb CORS spatial location.

4. Datasets and Processing Strategy

The GNSS observations for this station can be obtained by request from Zomba Geological Survey Office or from the University NAVSTAR Consortium (UNAVCO) at https://www.unavco.org/. UNAVCO is sponsored by the National Science Foundation (NSF) and the National Aeronautics and Space Administration (NASA) to provide services at no cost to support research world-wide.

To perform a thorough evaluation of pseudorange multipath for Zomba Geodynamics CORS in Malawi, seven (7) days observations, from **d**ay **o**f the **y**ear (DOY) 001 to DOY 007 of the month of January in 2018 were obtained from UNAVCO. The period of the GNSS datasets is within the recent configuration of the Trimble NETRS as depicted in Table 1. Seven days Receiver Independent Exchange Format (RINEX) 24-hour data were processed four (4) times in TEQC at 10º, 15º, 20º, and

25º cut-off angles above the horizon (Table 2). In TEQC, this horizon is simply a level plane parallel to the ellipsoid through the receiver's antenna.

Table 2: Processing parameters for pseudorange multipath.

Parameter	Setting
Constellation	GPS-Only
Frequency	L1 and L2
Elevation Mask (Cut-off)	10º; 15º; 20º, and 25º
Sampling	15 Seconds
Time Line Window Length	24.00 Hour(s), Ticked every 3.0 Hour(s)

The linear combinations in equations [13] and [14] were used to compute MP1 and MP2 multipath effects at these four elevation masks, respectively. This was done to detect the noise caused by the sources of electromagnetic radiation at the defined elevation angles on MP1 and MP2 for the selected days. Thus, the average Root Mean Square (RMS) values of MP1 and MP2 were determined. To better analyse the pseudorange multipath, the receiver Signal to Noise Ratios (SNR1 and SNR2) were assessed with respect to SV sky paths (elevation and azimuths). As the name suggests, SNR denotes a ratio of signal power to the noise floor of the GNSS observation and is used to map the multipath around an antenna. Furthermore, the number of SVs affected by each cut-off-angle reflector and the overall Geometric Dilution of Precision (GDOP) for the station were computed for each DOY.

5. Results and Analysis

5.1. Pseudorange Multipath

The average RMS values for MP1 and MP2 linear combinations of the pseudorange observations are presented in Figure 2 and Figure 3. These define the L1 pseudorange multipath for C/A or P-code observations and the L2 pseudorange multipath for P-code GNSS observations, respectively. As can be seen, the dark-blue, sky-blue, green, and yellow bars represent 10º, 15º, 20º, and 25º elevation masks, respectively (Figure 2 and Figure 3).

It is evident from MP1 and MP2 illustration that pseudorange multipath decreases with increase in cut-off angles. In both cases, average pseudorange multipath at elevation mask of 10º and 25º is the highest and least, respectively. This is attributed to the fact that satellite signals at low elevation angles are susceptible to the sources of electromagnetic radiation. Already, the GNSS signals for satellites in the horizon take a longer path to reach the receiver. As these signals encounter obstructions such as trees and towers, (Figure 1) the path is lengthened further (Braasch and Van Dierendonck, 1999). This eventually weakens the signal power that takes the indirect path more than that of the direct path (Kalyanaraman et al., 2004). This explains why the low-elevation-angle multipath is higher than that of the high-elevation.
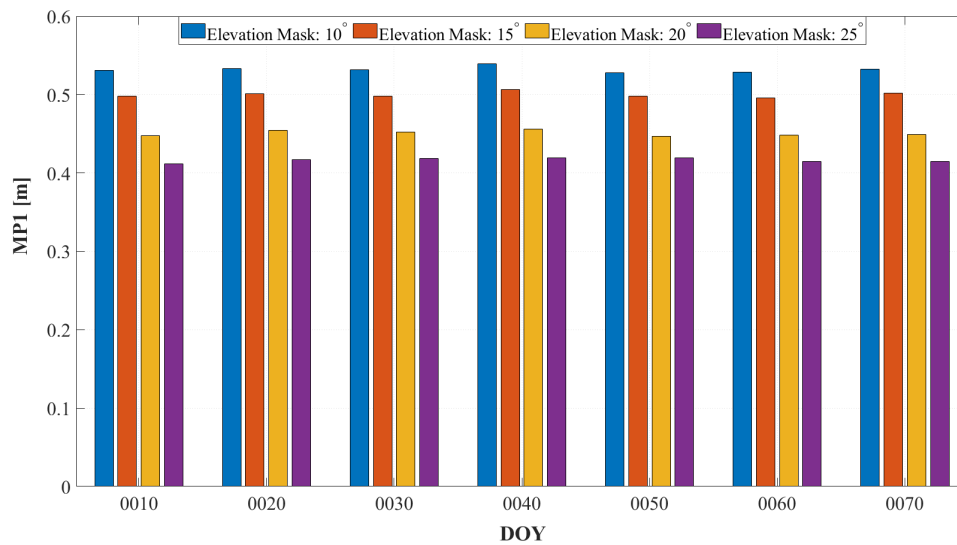
Figure 2: Pseudorange multipath on L1 for the selected days.

Despite the variations in multipath with respect to elevation angles, Figure 2 demonstrates less pseudorange multipath effects on L2 than on L1. The average RMS value for MP2 at 10º elevation mask is about 0.40 meters and above 0.50 meters for MP1. Statistics for the station reveals minimum RMS values of 0.41 m and 0.30 m for MP1 and MP2, respectively.
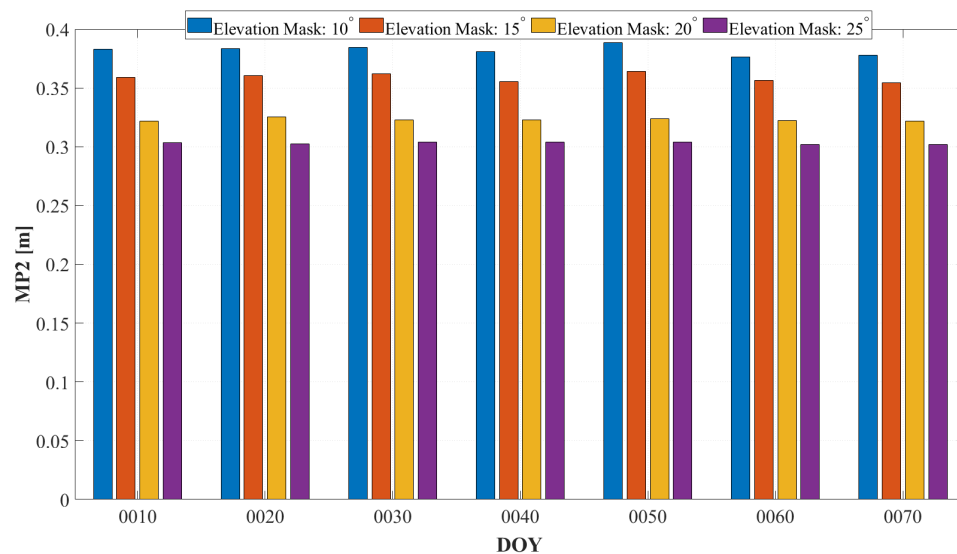
Figure 3: Pseudorange multipath on L2 for the selected days.

The elevation mask of 25º yields the least MP1 and MP2 multipath effects of all the cut-off angles for Zomba geodynamics CORS. However, the station has more MP1 multipath effects than MP2 at all the elevation cut-off angles. In addition, the MP1 and MP2 pseudorange multipath computed for the seven days are, however, worse at the first two elevation masks of 10º and 15º than at the other elevation angles. At these cut-off angles, the multipath effects are above the acceptable limit of 0.35 m (Munghemezulu, 2013). For the two elevation angles (10º and 15º), MP1 and MP2 multipath computed at 10º is worse as can be seen in Table 3. This may be attributed to the fact that the CORS is on the roof-top, close to a tall tree and transmission tower. The computed multipath effects at 10º

elevation angle are depicted in Figure 4. Furthermore, MP1 and MP2 pseudorange multipath effects are within the acceptable tolerance at elevation masks of 20º and 25º. Between these two angles (20º and 25º), the cut-off angle of 25º has low pseudorange multipath effects (Table 3).

Table 3: Multipath statistics with respect to elevation mask for the selected days.

	Elevation Mask:10 º		Elevation Mask:15 º		Elevation Mask:20 º		Elevation Mask:25 º	
	Min	Max	Min	Max	Min	Max	Min	Max
MP1(m)	0.527657	0.539550	0.495443	0.506590	0.446865	0.455617	0.411325	0.419512
MP2 (m)	0.376448	0.388589	0.354303	0.363876	0.321731	0.325365	0.301794	0.303967
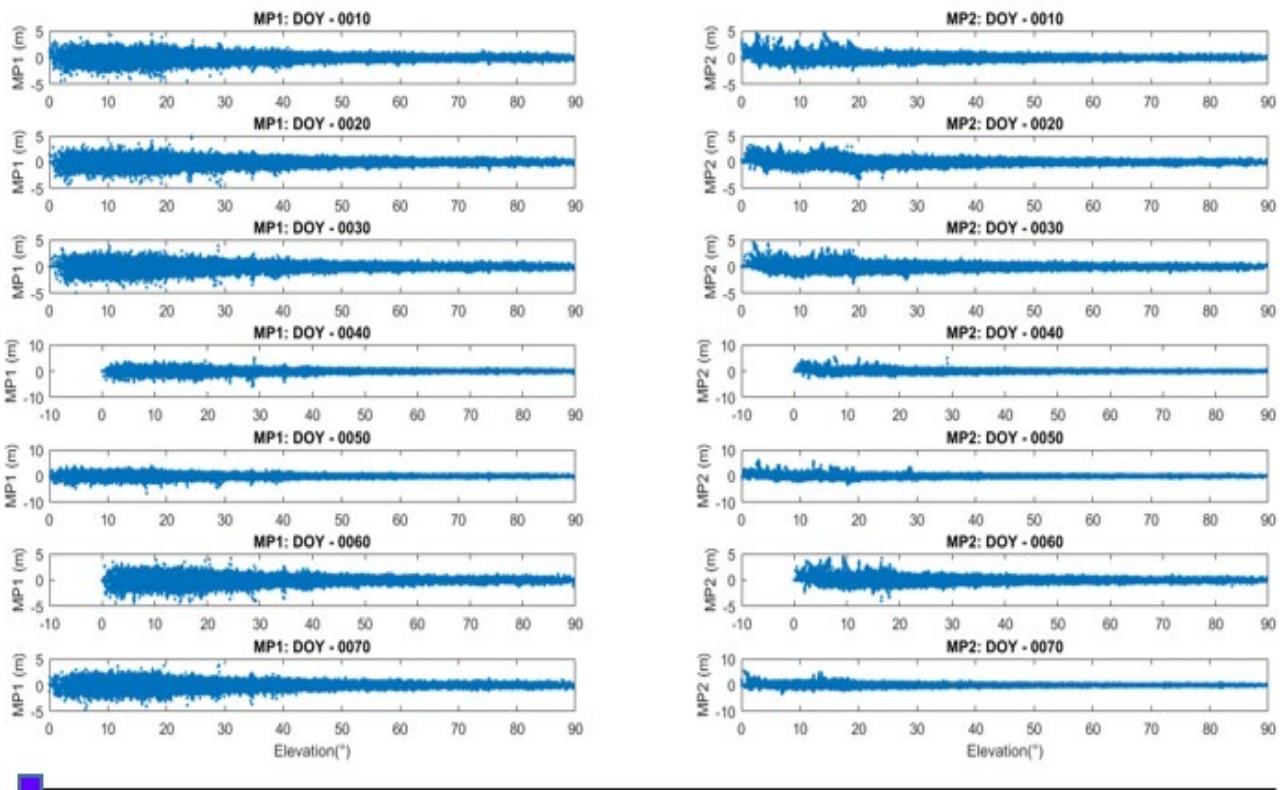
Figure 4: Pseudorange multipath (MP1 and MP2) against elevation.

5.2. Signal to Noise Ratio

The SNR1 and SNR2 for the selected days were computed and the statistical results are presented in Table 4. The SNR1 and SNR2 are plotted for each day as illustrated in Figure 5 which shows an increase in both SNR1 and SNR2 with respect to elevation angle.

Table 4: SNR statistics with respect to elevation mask for the selected days.

	Elevation Mask:10 º		Elevation Mask:15 º		Elevation Mask:20 º		Elevation Mask:25 º	
	Min	Max	Min	Max	Min	Max	Min	Max
SNR1(dBHz)	46.21	46.31	46.93	47.03	48.00	48.10	48.81	48.92
SNR2(dBHz)	34.62	34.86	35.61	35.87	37.26	37.53	38.72	39.00
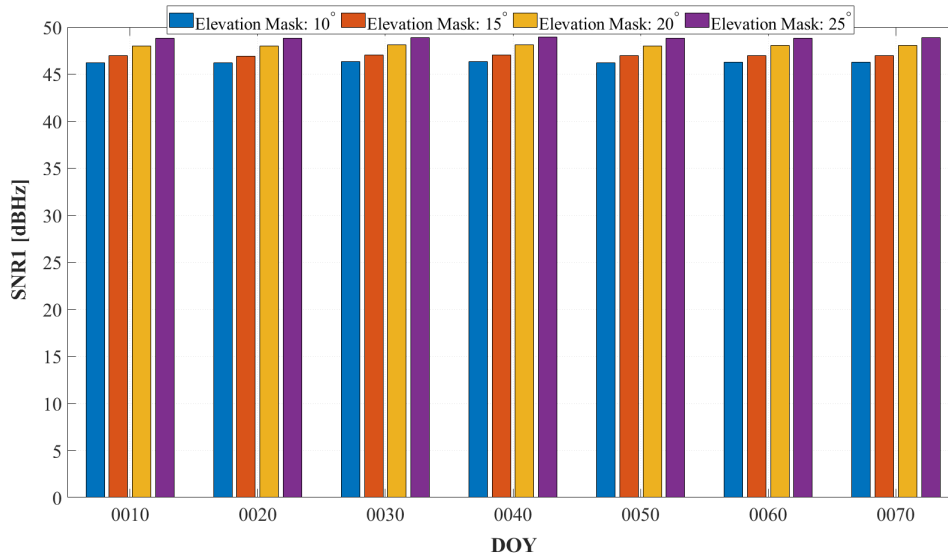
Figure 5: SNR1 for the selected days.
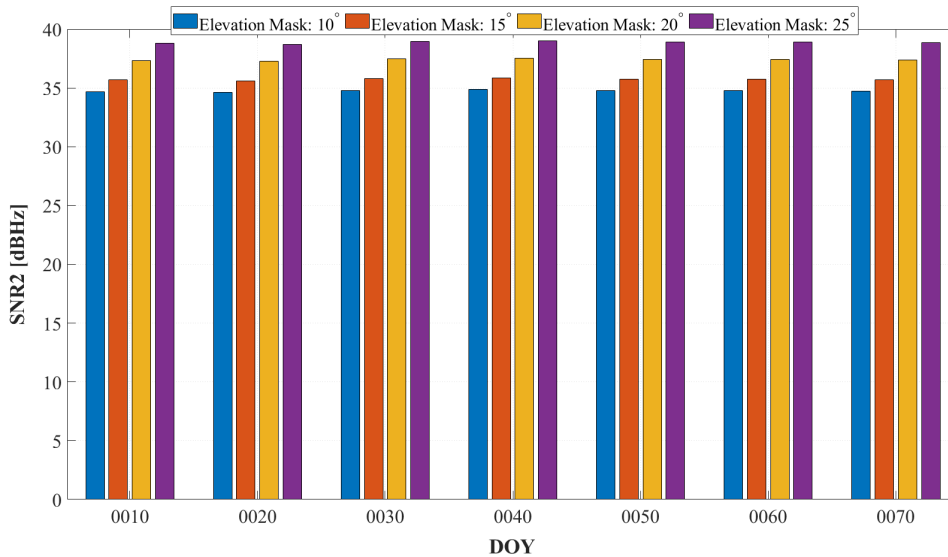
Figure 6: SNR2 for the selected days.

Moreover, the statistics reveal that the SNR2 has smaller noise values than SNR1. This is also true according to the SNR1 and SNR2 plots against elevation mask 10º depicted in Figure 7. In an interference-free environment, an appropriate antenna should provide a SNR of above 42 dBHz (Groves, 2013). For the selected days, the SNR1 are between 40 dBHz and 50 dBHz (Figure 5) whereas those of SNR2 are between 30 dBHz and 40 dBHz (Figure 6). Since SNR measures signal strength in presence of noise (Hetet & Langley, 2000), then the SNR2 values are weak (less than 42 dBHz) in all seven days. To be within acceptable tolerance, the SNR1 values should approximately range from 30 to 40 dBHz at low elevations (less than 60º) and 50 to 55 dBHz above 60º (Estey and Wier, 2013). For Zomba geodynamics CORS, the magnitude of SNR1 is considerably not bad with respect to the typical values (Figure 7).
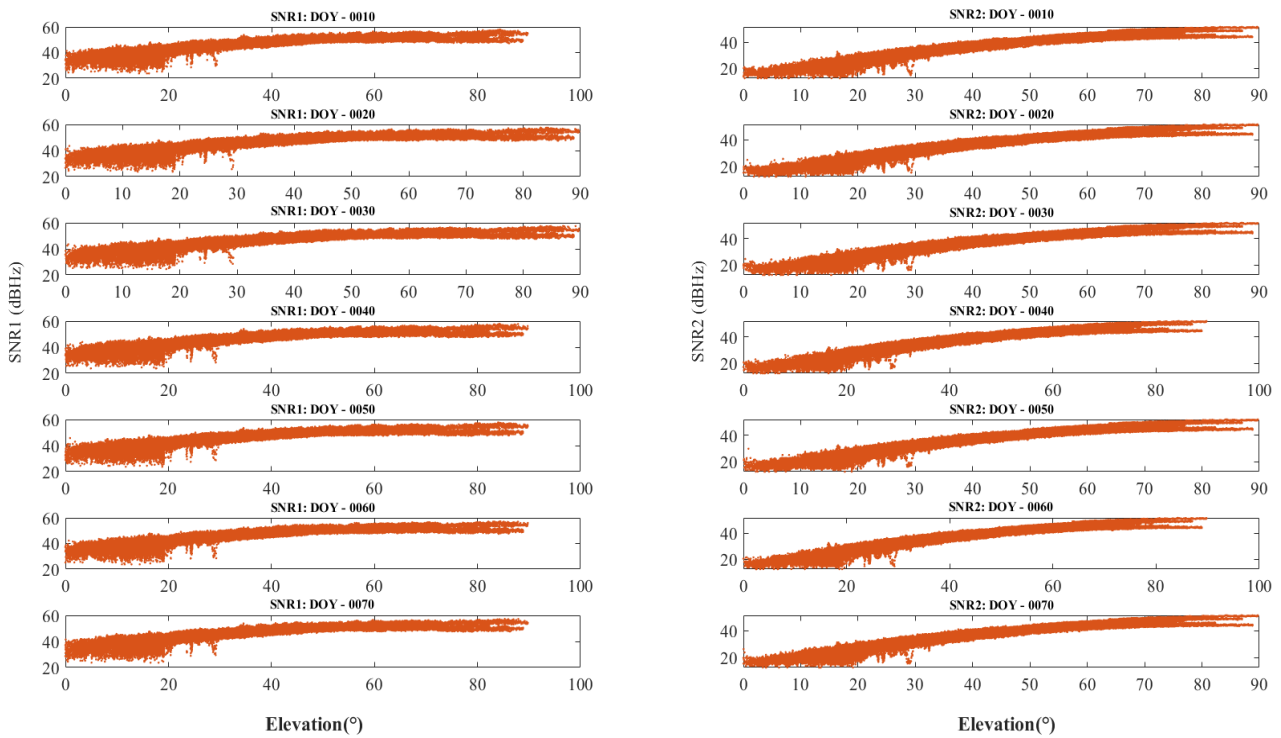
Figure 7: SNR1 and SNR2 against elevation angles.

5.3.   SVs and GDOP

To define and obtain a precise position, velocity, and timing at the user location by GNSS, there should be a minimum of four satellites. The number of SVs increases with an increase in navigation systems. However, in a single-system GNSS, the number of SVs required to fix a position may be affected by the elevation angle needed at post-processing of GNSS observations.
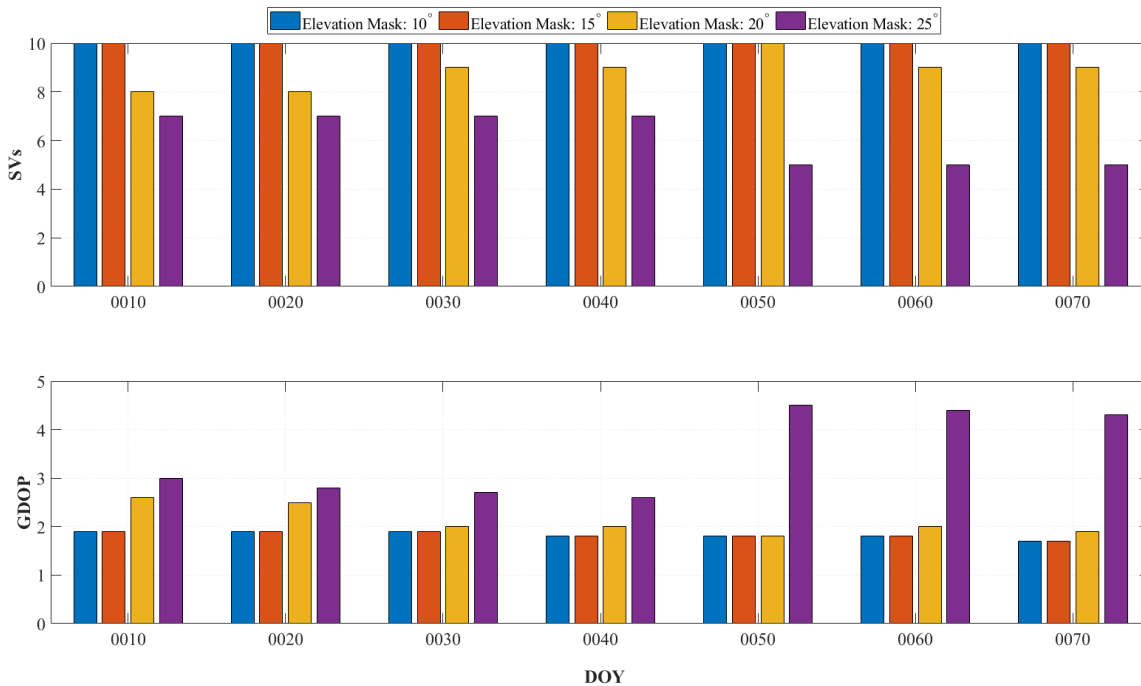
Figure 8: Number of Satellites and GDOP.

In the course of computing multipath at distinct cut-off angles, some satellites are eliminated from the total number of observed SVs. In this paper, the number of SVs at each elevation angle is presented in Figure 6. As can be seen, the maximum and minimum number of SVs for the selected days is ten (10) and five (5), respectively. This number of SVs is true for all the days at elevations angles of 10º and 15º. Similarly, the same number of SVs were observed on DOY 0050 at elevation angle of 20º. The least number of satellites (5) is observed at elevation angle of 25º. Sky-plots were used to distinguish the satellite configuration at elevation masks of 10º and 25º on DOY 0050 (Figure 9) to demonstrate the relation between cut-off angle and satellite visibility.

It is apparent that the decrease in the number of observed SVs significantly increases the average GDOP for the station (Figure 8). The best average GDOP of 1.7 is at elevation angles 10º and 15º on DOY 007 at which ten satellites were tracked. The poorest mean GDOP of 4.5 was recorded for DOY 0050 at elevation angle of 25º. This follows that elevation angle of 25º outperforms all other elevation angles in reducing pseudorange multipath at Zomba geodynamics CORS. However, the number of SVs observed at this elevation angle (25º) decreases which eventually increases GDOP value. This is indicated by an increase of about 38% in GDOP from 1.7 to 4.5 (at 10 º and 15 º, and 25 º, respectively). The number SVs reduces to five which is above the minimum number of four required to define a position by GNSS.
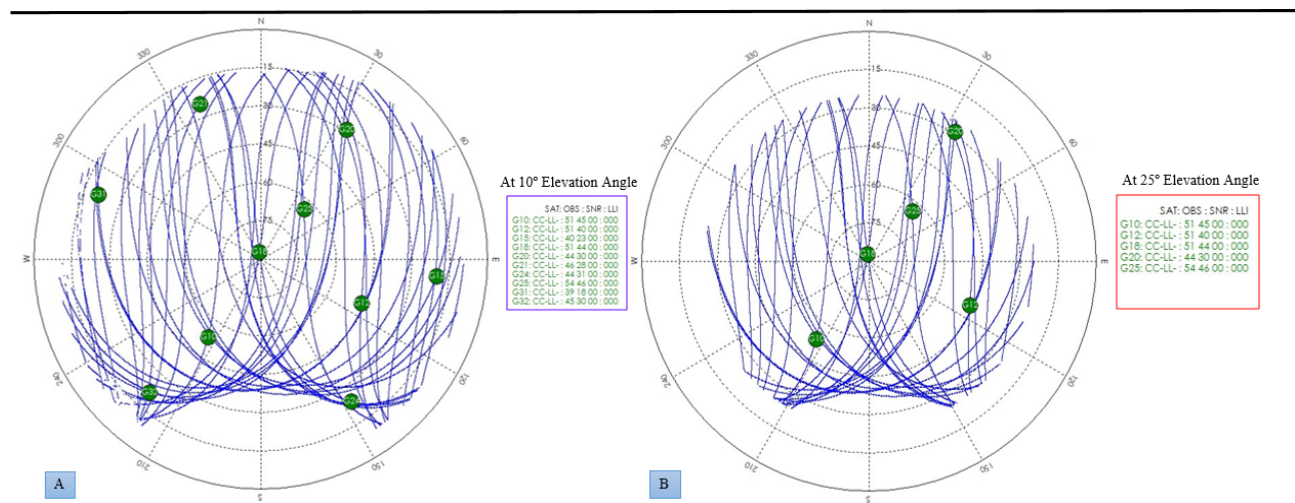
KEY: The skyplot labelled A was generated at an elevation mask of 10 degrees. The skyplot B was generated at an elevation mask of 25 degrees. The observed satellites are summarised in the sky-blue and red boxes.

Figure 9: Sky-plot at 10º and 25º elevation mask on DOY 0050 in 2018.

6. Conclusions

Multipath is one of many error sources affecting GNSS positioning accuracy. The impact of multipath is characterized in the context of a given environment and application. This paper evaluated pseudorange multipath and Signal Noise Ratio (SNR) on both L1 and L2 for Zomba geodynamics CORS, in Malawi. Zomba CORS is the only continuous GPS station in the southern region of Malawi located at the roof-top of Zomba Geological Survey Headquarters premises purposefully to be used for geodynamics experiments. One-week GNSS observations spanning a twenty-four hour interval

for DOY 001 to DOY 007 in January 2018 were analysed in TEQC software at four different elevation cut-off angles.

Besides computing multipath at different elevation angles, the number of SVs and GDOP were also determined for the station. Results indicate high multipath effects (above the acceptable limit of 0.35m) in both MP1 and MP2 at 10º elevation mask among the four different angles. The least MP1 and MP2 multipath effects were detected at an elevation angle of 25º in all the selected days. In addition, MP1 multipath was worse than MP2 all the angles. The SNR1 and SNR2 for the selected days were computed and the statistical results indicate an increase in both SNR1 and SNR2 with respect to elevation angle. For these days, L2 signal was more affected by noise than L1. Further to this, an assessment of SVs and GDOP for Zomba CORS show that at least ten (10) satellites were observed in each day 10º and 15º elevation cut-off. The number of satellites dropped to five (5) at the elevation angle of 25º. This number of satellites (5) is still more than required to position fixing by GNSS. On the contrary, five satellites at this angle (25º) resulted into a larger GDOP value of 4.5, an increase in GDOP by about 38% (from 1.7 at 10º and 15º elevation cut-off). Furthermore, the number of satellites drop by half (from 10 to 5), then the station has to be upgraded to a multi-constellation CORS by including other navigation systems such as GLONASS, Galileo and BeiDou. This can increase both the number of satellites and precision.

Multipath between the GNSS satellite and receiver repeats every sidereal day. Since multipath is azimuth and elevation dependent, it therefore demonstrates the same pattern between consecutive days. Consequently, such a repetition may be used to model the multipath at a given GNSS receiver. While it is essential not to observe satellites close to the horizon in order to reduce multipath, it is also recommended that multipath be modelled or removed using modern post-processing software for Zomba geodynamics GNSS observations. Thus, all satellites below 15º cut-off angle be excluded from post-processing Zomba geodynamics GNSS datasets. This study has gathered that satellites below this angle are highly affected by code multipath and the signal strength is weak. Since multipath occurs when part of the satellite signal reaches the GNSS receiver after encountering reflections of scattering from the near-by features (such as the ground, buildings, and trees), it is recommended that trees very close to the CORS antenna be removed.

7. Acknowledgement

8. References

Abidin, HZ, Subarya, C, Muslim, B, Adiyanto, FH, Meilano, I, Andreas, H and Gumilar, I 2010, 'The Applications of GPS CORS in Indonesia: Status, Prospect and Limitation', in Proceedings of the FIG Congress, *TS 4C - GNSS CORS Networks - Infrastructure, Analysis and Applications II*, Sydney, Australia, 11-16 April 2010.

Bilich, A & Larson, KM 2007, 'Mapping the GPS multipath environment using the signal-to-noise ratio (SNR)', *Radio Science*, vol. 42, no. 6, pp. 1-16.

Bilich, A, Axelrad, P, and Larson, K 2007, 'Scientific Utility of the Signal-to-Noise Ratio (SNR) Reported by Geodetic GPS Receivers', *in Proceedings of 20th International Technical Meeting of the Satellite Division of The Institute of Navigation (ION GNSS 2007)*, Fort Worth, Texas, September 2007, pp. 1999-2010.

Bilich, A, Larson, KM, and Axelrad, P 2004, 'Observations of Signal-to-Noise Ratios (SNR) at Geode- tic GPS Site CASA : Implications for Phase Multipath', *in Proceedings of the Centre for European Geodynamics and Seismology*, vol. *23*, pp. 77–83.

Braasch, MS & Van Dierendonck, AJ 1999, 'GPS Receiver Architectures and Measurements', *in Proceedings of the IEEE*, vol. 87, no. 1, viewed 11 December 2018, <https://ieeexplore.ieee.org/stamp/stamp.jsp?tp=&arnumber=736341>.

Dammalage, T 2017, 'Analysis of Pseudorange-Based DGPS after Multipath Mitigation', *International Journal of Scientific and Research Publications,* Vol. 7, no. 11, pp. 77–84.

Estey, L & Wier, S 2013, 'Teqc Tutorial', *Basics of Teqc Use and Teqc Products*, UNAVCO, Boulder, Colorado U.S.A., Viewed 6 June 2014. <http:// www.unavco.org>.

Estey, LH & Meertens, CM 1999, 'TEQC: The multipurpose toolkit for GPS/GLONASS data', *GPS solutions*, vol. 3, no. 1, viewed 1 July 1999, pp. 42-49, <https://doi.org/10.1007/PL00012778>.

Groves, PD 2013, *'Principles of GNSS, Inertial, and Multisensor Integrated Navigation Systems'*, 2nd edition, Artech House, Boston.

Hetet, S, & Langley, SRB 2000, 'Signal-to-Noise Ratio Effects on the Quality of GPS Observations', *Analysis*.

Hilla, S & Cline, M 2004, 'Evaluating pseudorange multipath effects at stations in the National CORS Network'. *GPS Solutions*, vol. 7, pp. 253-267.

Hoffman-Wellenhof, B, Licthenegger, H & Collins, J 1994, *Global Positioning System: Theory and Practice*, 4th edition, Springer, Berlin, Germany

Hsu, LT, Jan, SS, Groves, PD, & Kubo, N 2015, 'Multipath mitigation and NLOS detection using vector tracking in urban environments' *GPS Solutions*. vol. 19, pp. 249-262.

Irsigler, M 2010, 'Characterization of multipath phase rates in different multipath environments', *GPS Solutions*, vol. 14, no. 4.

Joseph, A 2010, 'GNSS Solution: Measuring GNSS Signal Strength', *Inside GNSS*, viewed December 2017, pp.20–25, <http://www.insidegnss.com/auto/novdec10-Solutions>.

Kalyanaraman, SK, Kelly, JM, Braasch, MS and Kacirek, J 2004, 'Influence of

GPS Code Tracking on Multipath Performance', in *Proceedings of IEEE Aerospace Conference*, Big Sky, MT, March 2004, pp. 1677-1686, IEEE, USA, 2004.

Kildal, PS, Orlenius, C, & Carlsson, J. 2012, 'OTA testing in multipath of antennas and wireless devices with MIMO and OFDM', in *Proceedings of the IEEE*. Vol. 100, no. 7, Viewed September 2017, pp. 2145-2157,< https://doi.org/10.1109/JPROC.2012.2188129>.

Krantz, E, & Riley, S and Large, P 2001, 'The Design and Performance of the Zephyr Geodetic Antenna', in *Proceedings of the 14th International Technical Meeting of the Satellite Division of The Institute of Navigation (ION GPS)*, Salt Lake City, Utah, September 2001, pp. 1942-1951, ION GPS, Utah, 2001.

Lakmal, T 2018, 'Effects of Site-Dependent Errors on the Accuracy of C/A Code DGPS Positioning' *Civil Engineering Journal*, vol. 4, no. 10, pp. 2296-2304.

Lau, L, & Cross, P 2007, 'Development and testing of a new ray-tracing approach to GNSS carrier-phase multipath modelling', *Journal of Geodesy*, Vol. 81, no. 11, pp. 713-732.

Leick, A, Rapoport, L, & Tatarnikov, D 2015, *GPS Satellite Surveying,* 4th edition, Wiley, USA.

Lentmaier M, Krach B, Jost T, Lehner A, and Steingass A 2007, 'Assessment of multipath in aeronautical environments', in *Proceeding of 11th European Navigation Conference*, Geneva, Switzerland, May-June 2007, pp 2-12, Geneva, 2007.

Munghemezulu, C 2014, 'Determination of geodetic velocity field parameters for the African tectonic plate using the technique of Global Navigation Satellite Systems', *Msc Dissertation*, Graduate Faculty of the University of Pretoria, December 2014.

Munghemezulu, C, Combrinck, L, Botai, J, & Mashaba, Z 2016, 'Mapping GPS Multipath : a Case Study for the Lunar Laser Ranger Timing Antenna at HartRAO, *South African Journal of Geomatics*, vol. 5, no. 2, pp. 142-155.

Park, KD, Nerem, RS, Schenewerk, MS, & Davis, JL 2004, 'Site-specific multipath characteristics of global IGS and CORS GPS sites', *Journal of Geodesy*, vol. 77, pp. 799-803.

Phan, QH, Tan, SL, & McLoughlin, I 2013, 'GPS multipath mitigation: A nonlinear regression approach', *GPS Solutions*, vol. 17, no. 3, pp. 371-380.

Preston, S 2015, 'GPS Multipath Detection and Mitigation Timing Bias Techniques', *MSc Dessertation*, Graduate Faculty of Auburn University.

Webb, SL 1997, 'Lecture Notes in Earth Sciences', *Lecture Notes in Earth Sciences, vol 67*.

Wieser, A, & Brunner, F 2002, 'SIGMA-F: Variances of GPS observations determined by a Fuzzy system', in Ádám J and Schwarz KP (eds.), *Vistas for Geodesy in the New Millennium, international Association of Geodesy Symposia*, Hungary, September 2001, pp. 365-370, Springer, Berlin, Heidelberg, <http://link.springer.com/chapter/10.1007/978-3-662-04709-5_60>.

Yuan, M, Li, D, Li, B, Chen, H, & Ou, G, 2017, 'Assessment Method of Multipath Mitigation Performance for GNSS Antenna with Receiver Algorithms,' *International Journal of Antennas and Propagation*, vol. 2017, no. 3, pp. 1-13.

Zavorotny, VU, Larson, KM, Braun, JJ, Small, EE, Gutmann, ED, & Bilich, AL 2010, 'A Physical Model for GPS Multipath Caused by Land Reflections: Toward Bare Soil Moisture Retrievals', *IEEE Journal of Selected Topics in Applied Earth Observations and Remote Sensing*, vol. 3, no. 1, viewed March 2010, pp. 100-110, https://ieeexplore.ieee.org/document/5290072 >.